



Research Article

Monitoring Instantaneous Dynamic Displacements of Masonry Walls in Seismic Oscillation Outdoors by Monocular Digital Photography

Guojian Zhang ^{1,2}, Guangli Guo ^{1,2}, Chengxin Yu ³, Long Li ^{2,4},
Sai Hu ² and Xue Wang ²

¹NASG Key Laboratory of Land Environment and Disaster Monitoring, China University of Mining and Technology, Daxue Road 1, Xuzhou 221116, Jiangsu, China

²School of Environmental Science and Spatial Informatics, China University of Mining and Technology, Daxue Road 1, 221116 Xuzhou, Jiangsu, China

³Business School, Shandong Jianzhu University, Fengming Road 1000, 250101 Ji'nan, Shandong, China

⁴Department of Geography, Vrije Universiteit Brussel, Pleinlaan 2, 1050 Brussels, Belgium

Correspondence should be addressed to Guangli Guo; guo_gli@126.com

Received 18 May 2018; Revised 24 July 2018; Accepted 26 July 2018; Published 7 August 2018

Academic Editor: Arkadiusz Zak

Copyright © 2018 Guojian Zhang et al. This is an open access article distributed under the Creative Commons Attribution License, which permits unrestricted use, distribution, and reproduction in any medium, provided the original work is properly cited.

Understanding the development of cracks in masonry walls can provide insight into their capability for earthquake resistance. The crack development is characterized by the displacement difference of the adjacent positions on masonry walls. In seismic oscillation, the instantaneous dynamic displacements of multiple positions on masonry walls can warn of crack development and reflect the propagation of the seismic waves. For this reason, we proposed a monocular digital photography technique based on the PST-TBP (photographing scale transformation-time baseline parallax) method to monitor the instantaneous dynamic displacements of a masonry wall in seismic oscillation outdoors. The seismic oscillation was simulated by impacting a suspended steel plate with a hammer and by simulation software ANSYS (analysis system), for comparative analysis. The results show that it is feasible to use a hammer to impact a suspended steel plate to simulate the seismic oscillation as the stress concentration zones of the masonry wall model in ANSYS are consistent with the positions of destruction on the masonry wall, and that the crack development of the masonry wall in the X-direction could be characterized by a sinusoid-like curve, which is consistent with previous studies. The PST-TBP method can improve the measurement accuracy as it corrects the parallax errors caused by the change of intrinsic and extrinsic parameters of a digital camera. South of the test masonry wall, the measurement errors of the PST-TBP method were shown to be 0.83mm and 0.84mm in the X- and Z-directions, respectively, and in the west, the measurement errors in the X- and Z-directions were 0.49mm and 0.44mm, respectively. This study provides a technical basis for monitoring the crack development of the real masonry structures in seismic oscillation outdoors to assess their safety and has significant implications for improving the construction of masonry structures in earthquake-prone areas.

1. Introduction

The magnitude, 7.9 Wenchuan earthquake of 2008, occurred along the Longmenshan Fault with an 11-degree epicenter intensity [1]. The earthquake was felt across China and was profiled as the strongest earthquake in China since 1949. Statistics show that this destructive earthquake knocked down ~6,500,000 houses and destroyed ~23,000,000. More than 80% of the structures affected were masonry houses

[2]. Rapid house collapse led to numerous inhabitants buried and thus killed. The catastrophic consequences have offered clear evidence of the poor performance of those masonry structures during the earthquake attack. Since then, Chinese authorities at all levels have been implementing strict policies and rules on the resistance of buildings to earthquakes. The seismic resistance of masonry structures has therefore become a hotspot once again in recent years in China and beyond.

A crack in masonry structures caused by earthquake load is a common problem that needs to be solved. Monitoring crack development in masonry walls has important significance in the study of the earthquake resistance capability of masonry structures [3]. As seismic oscillation is an extremely complex process, the crack development mechanism of masonry structures is not clear and there is no precise mathematical model to describe the change characteristics. Examining the current literature, most scholars adopt a structure test to study crack development in a masonry structure [4]. A few analyze masonry structure with consideration of an earthquake or dynamic load as a model. As finite element models emerged, Arne [5] and Pietro [6] have successfully simulated masonry structure in seismic oscillation. However, the finite element method gradually becomes invalid in studying the crack development mechanism with the increase of the crack development of the masonry walls. The finite element method can reproduce the process of seismic oscillation well and reflect the influence of strain rate when a shaking table shakes, and the method is useful for studying the masonry walls in seismic oscillation. Some researchers also used shaking tables to study the failure pattern, dynamic response, and collapse mechanism of masonry structures [7]. Using shaking tables for large scale masonry structures is, however, challenging due to the limited bearing capacity and size of the tables. And the shaking table is too expensive to be a conventional method to study the crack development of masonry walls in seismic oscillation. This study used a hammer to impact a suspended steel plate to simulate the seismic oscillation in the field.

Few techniques and methods are available to monitoring the crack development of masonry walls in seismic oscillation in the field. The techniques and methods currently available are not effective in continuously monitoring the instantaneous dynamic displacements of masonry walls in seismic oscillation in the field. This problem can be solved, however, by applying monocular digital photography. Monocular digital photography, combining photogrammetric technique with information technology, presents an opportunity to monitor the instantaneous dynamic displacement of engineering structures by adopting a nonmetric digital camera to observe multiple points simultaneously and to capture the instantaneous displacement of a deformable object [8]. Although digital photography has not been as popular in engineering structures as in other fields such as biomechanics, chemistry, biology, and architecture, many pioneering applications in this field have demonstrated its underestimated potential, e.g., for monitoring bridge structures [9–11], structural cracks [12–15], and masonry wall displacements with digital image correlation (DIC) method [3, 16–20]. Moreover, the DIC method is also used to monitor the strain development on bricks [21]. These examples demonstrate that it is feasible to monitor the masonry walls to examine the crack development pattern in seismic oscillation with monocular digital photography.

The DIC method, which is popular for studying the crack development of a masonry wall in the laboratory, needs a special light source for the test. The light cannot be projected evenly onto the structure when monitoring large engineering

structures, resulting in low measurement accuracy, which is even lower outdoors as higher light quality is required.

The objective of this study is to propose monocular digital photography based on the PST-TBP (photographing scale transformation-time baseline parallax) method [22, 23] to monitor the instantaneous dynamic displacements of masonry walls in seismic oscillation outdoors. Based on the monitoring data obtained through the technique, we analyzed the influence of the S-wave (shear wave) on masonry walls in seismic oscillation and investigated the relationship between the crack development pattern and the seismic wave propagation on the masonry wall. Monocular digital photography based on the PST-TBP method can even be used to monitor the real masonry house in seismic oscillation to warn of the possible danger.

2. Monocular Digital Photography

Both the DLT (direct linear transformation) method [24] and the PST-TBP (photographing scale transformation-time baseline parallax) method [25] can be used to process the image sequences. The DLT method requires at least six reference points, which should be evenly distributed and encircle the target. In addition, their spatial coordinates need to be accurate enough for allowing the calculation of the spatial coordinates of deformation points [26]. These requirements are, however, difficult to achieve outdoors. As a result, the DLT method is often used to monitor small objects in the laboratory. The PST-TBP method was therefore used in this study. In this method, the reference points are used to match a zero image with successive images. Their placements are not as strict as in the DLT method. It is not essential to obtain the spatial coordinates of the reference points because the object is to obtain the relative displacement of the targets.

2.1. Distortion Correction of Nonmetric Digital Cameras. The distortion of the camera used in photography contributes to a decrease in the measurement accuracy [27, 28]. The distortion error is linear near the center of the images in a short photographing distance when the digital camera and the monitored object do not move in the test field [29]. Thus, we adopted a grid-based method [30] in the study to eliminate the distortion of the digital camera (detailed in Section 2.3). Figure 1 illustrates that the distortion error of the feature point on the monitored object moves from Position A to Position A' in the camera's view and that ΔX and ΔZ are the corresponding horizontal and vertical values.

The steps to correct the distortion error by a grid are as follows: first, a grid was fixed at a photographing distance S from a SONY350 digital camera (Figure 2 and Table 1) to the grid plan. The photographing distance was recorded, and the corresponding photos of the grid were taken. Second, we compared the highest quality photo of the grid to the real grid without being affected by the distortion and carefully observed the feature points on the monitored object such as point A, to analyze the size and direction of the distortion. Third, the camera was removed along the photographing direction with the first and second steps reiterated. Last, a

TABLE 1: Technical parameters of the Sony-350 camera used in the study.

Type	Sensor	Sensor Scale	Focal length	Active pixels
Sony DSLR A350(Sony-350)	CCD	23.5×15.7mm	35mm(27-375)	4592×3056 pixels

TABLE 2: Spatial coordinates (/m) of reference points C0 to C7.

Point no.	C0	C1	C2	C3	C4	C5	C6	C7
X	108.343	109.739	110.144	110.144	109.492	108.862	108.456	108.713
Y	95.770	95.804	95.957	95.957	97.022	97.199	96.194	96.487
Z	99.534	99.542	99.540	99.540	99.568	99.240	99.225	99.384

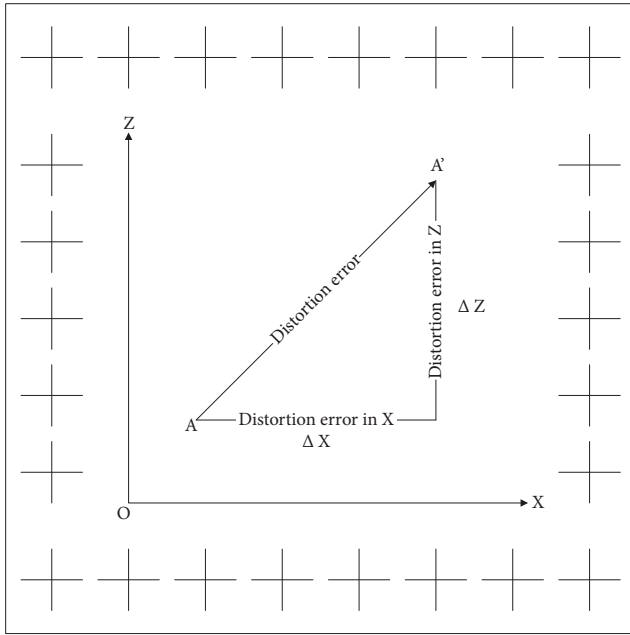


FIGURE 1: Analysis of distortion error through a 50cm×50cm grid.

mathematical expression for eliminating the distortion was therefore formulated.

After correction, the DLT method was used to assess the measurement accuracy of the digital camera. We measured the spatial coordinates of the reference points and deformation points in relation to the total station position in the laboratory for ease of calculation (Table 2). Taking the top left corner of an image as the origin of the pixel coordinate system, we recorded their pixel coordinates in relation to the origin position (Table 3). The DLT method was used to calculate the spatial coordinates of deformation points U0 and U1 based on the coordinates in Tables 2 and 3. Their differences were obtained by comparing the actual coordinates of U0 and U1 with their calculated coordinates (Table 4). The actual coordinates were the spatial coordinates of deformation points monitored by a total station, and the calculated coordinates were the spatial coordinates of deformation points calculated by the DLT method.

The maximal and minimal measurement errors were 2 mm and 0 mm, respectively, with an average measurement error of 1 mm, suggesting that the digital camera used in

this study meets the accuracy requirements of deformation observation.

2.2. Principle of Photographic Scale Transformation. The photographing scale of somewhere is always changing along the photographing distance (from the position to the photographing center) [31, 32]. Figure 3 shows a schematic diagram of a CCD (charge coupled device) camera capturing images at different photographing distances H3 and H4.

According to Figure 3, the relationship between pixel counts and distances can be described by

$$\frac{H1}{H2 + H3} = \frac{N}{D1} \quad (1)$$

$$\frac{H1}{H2 + H4} = \frac{N}{D2}$$

In general, H3 and H4 are meter-sized, while H2 is centimeter-sized. If H2 can be ignored when the camera is far from the bridge, (1) can be expressed as

$$\frac{H1}{H3} = \frac{N}{D1} \quad (2)$$

$$\frac{H1}{H4} = \frac{N}{D2}$$

From (2), we have

$$D2 = \frac{H4}{H3} \cdot D1 \quad (3)$$

Assume that M1 and M2 are the photographing scale of the reference plane and the object plane, respectively. According to (3), we have

$$M2 = \frac{H4}{H3} \cdot M1 \quad (4)$$

Namely,

$$M2 = \Delta PSTC \cdot M1 \quad (5)$$

where $\Delta PSTC$ is the photographing scale transformation coefficient and $\Delta PSTC = H4/H3$.

2.3. Photographing Scale Transformation-Time Baseline Parallax Method. If no errors exist in the measurement, the horizontal and vertical displacements on the object plane of a deformation point are given by



(a) Front view

(b) Side view

FIGURE 2: A Sony-350 camera used for the monocular digital photography.

TABLE 3: Pixel coordinates (/pixel) of reference points (C0 to C7) and deformation points (U0 and U1).

Point no.		C0	C1	C2	C3	C4	C5	C6	C7	U0	U1
Photo 1	X	205	428	581	958	1540	1864	782	1120	429	1541
	Z	687	468	437	451	490	924	1057	796	700	718
Photo 2	X	144	1179	1486	1716	1918	1631	487	907	619	1543
	Z	572	495	491	530	605	1101	948	799	643	826

TABLE 4: Accuracy assessment for deformation points U0 and U1.

Name	Actual coordinates/m	Calculated coordinates/m	Differences/mm
U0-X	108.825	108.826	1
U0-Y	95.887	95.888	1
U0-Z	99.441	99.440	1
U1-X	109.067	109.065	2
U1-Y	96.935	96.934	1
U1-Z	99.394	99.394	0

$$\begin{aligned}\Delta X^{PST} &= M \cdot \Delta P_{STC} \cdot \Delta P_x = M^{PST} \Delta P_x \\ \Delta Z^{PST} &= M \cdot \Delta P_{STC} \cdot \Delta P_z = M^{PST} \Delta P_z\end{aligned}\quad (6)$$

where ΔX^{PST} and ΔZ^{PST} are the horizontal and vertical displacements on the object plane of a deformation point, ΔP_x and ΔP_z are the horizontal and vertical displacements on the image plane of a deformation point, M is the photographing scale on the reference plane, and M^{PST} is the photographing scale on the object plane. ΔP_x and ΔP_z have parallax errors.

The PST-TBP method was however used to eliminate the errors caused by the change of intrinsic and extrinsic parameters of a digital camera. The PST-TBP method consists of three steps. First, the TBP method is used to obtain the displacements on the reference plane of a deformation point. These displacements have the parallax errors caused by the change of intrinsic and extrinsic parameters of a digital camera. Second, the reference points are used to match a zero image with the successive images to eliminate the parallax errors. The corrected displacements on the reference plane are obtained. Lastly, the real displacements of a deformation point are equal to its corrected displacements on the reference

plane multiplied by the photographing scale transformation coefficient. The details are as follows.

The first step, when a point on the object plane moves from A to B (Figure 4), the horizontal and vertical displacements on the reference plane of a deformation point are given by

$$\begin{aligned}\Delta X &= M \Delta P_x \\ \Delta Z &= M \Delta P_z\end{aligned}\quad (7)$$

where ΔX and ΔZ are the horizontal and vertical displacements on the reference plane of a deformation point, ΔP_x and ΔP_z are the horizontal and vertical displacements on the image plane of a deformation point, and M is the photographing scale on the reference plane. ΔP_x and ΔP_z have parallax errors

In the second step, some points are laid at a stable position around the camera to form a reference plane that is perpendicular to the photographing direction, and the parallax is therefore eliminated through differencing a zero image with the successive images based on a reference plane, respectively.

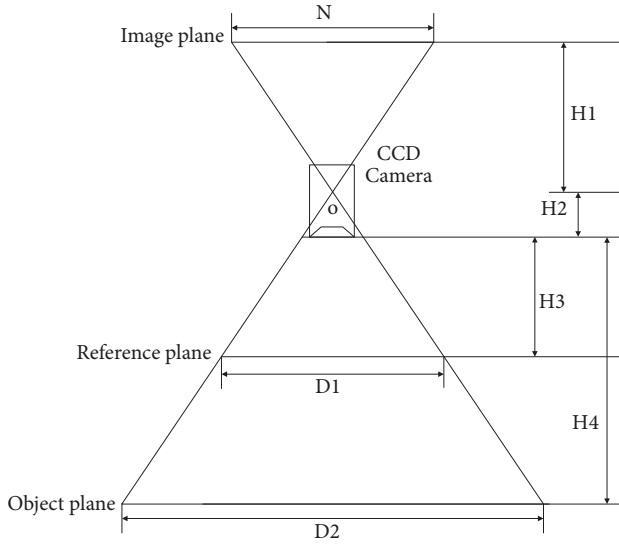


FIGURE 3: Schematic diagram of photographing scale transformation: H1 is the focal length of a CCD camera, H2 is the distance between the optical origin (o) and the front end of the CCD camera, D1 on reference plane and D2 on the object plane are the real-world lengths formed by the view field of the CCD camera at photographing distances H3 and H4, respectively, and N is the maximal pixel number in a horizontal scan line of an image plane, which is fixed and known a priori irrelevant to the photographing distances.

The reference plane in Figure 4 consists of six reference points labeled as C0-C5 (at least three reference points), and the reference plane equation can be expressed as

$$\begin{aligned} P_x &= a_x x + b_x z + c \\ P_z &= a_z x + b_z z + d \end{aligned} \quad (8)$$

where (x, z) and (P_x, P_z) are the image plane coordinates and the image plane parallaxes of a reference point, respectively; (a_x, b_x) and (a_z, b_z) are the parallax coefficients in the X- and Z- directions, respectively; and (c, d) are the constant parallax coefficients in the X- and Z- directions, respectively.

After correcting the pixel displacements on the image plane of a deformation point based on the parallaxes of the reference plane, the corrected pixel displacements on the image plane of a deformation point can be obtained:

$$\begin{aligned} \Delta P'_x &= \Delta P_x - P_x \\ \Delta P'_z &= \Delta P_z - P_z \end{aligned} \quad (9)$$

where $(\Delta P'_x, \Delta P'_z)$ and $(\Delta P_x, \Delta P_z)$ are the corrected pixel displacements and the measured pixel displacements on the image plane of a deformation point, respectively.

Then, we obtained the corrected displacements on the reference plane of a deformation point:

$$\begin{aligned} \Delta X' &= M \Delta P'_x \\ \Delta Z' &= M \Delta P'_z \end{aligned} \quad (10)$$

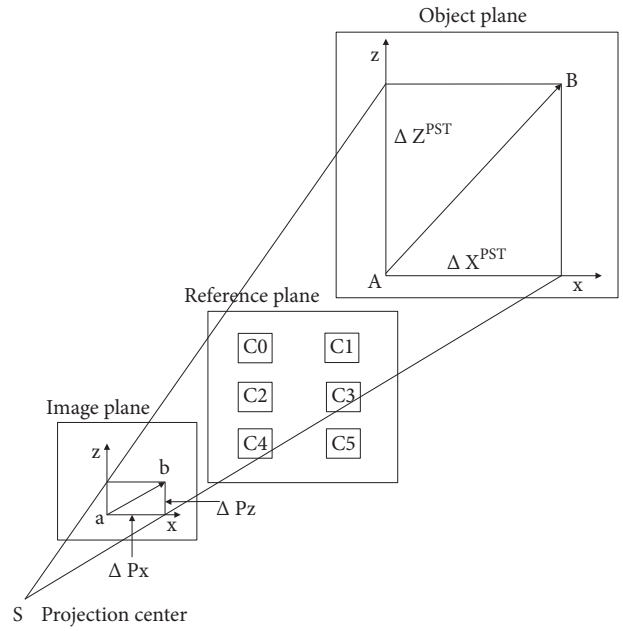


FIGURE 4: Photographing scale transformation-time baseline parallax (PST-TBP) method.

where $(\Delta X', \Delta Z')$ are the corrected displacements on the object plane of a deformation point.

In the last step, the real displacements on the object plane of a deformation point are given by

$$\begin{aligned} (\Delta X^{PST})' &= \Delta PSTC \cdot \Delta X' \\ (\Delta Z^{PST})' &= \Delta PSTC \cdot \Delta Z' \end{aligned} \quad (11)$$

where $(\Delta X^{PST})'$ and $(\Delta Z^{PST})'$ are the real displacements on the object plane of a deformation point.

To improve data processing speed, a data processing toolkit has been developed in the environment of Microsoft Visual C++ 6.0 that allows synchronization of measuring pixel coordinates of deformation points and data processing. The procedure of the toolkit is detailed in Figure 5. The PST-TBP method is the IM-TBP (image matching-time baseline parallax) method when $\Delta PSTC$ is 1 [33].

3. Masonry Wall Test in Seismic Oscillation

3.1. Test Preparation. Following the study of Sun [34], a masonry wall with an aspect ratio of 0.67 was used in our test. According to the test conditions and the corresponding design specifications [35], we adopted the Yishun Yiding method [36] to build a masonry wall (1.2m×0.8m×0.24m) with bricks (240mm×115mm×53mm) of cement mortar grade between M2.5 and M5.0 (Figure 6(a)) at a construction site where the foundation was being treated. The foundation soil was native, yellow, and compacted silt clay which was of strong compressive strength. A pit (2.1m×1.4m×0.2m) was dug on the foundation and a manganese steel plate

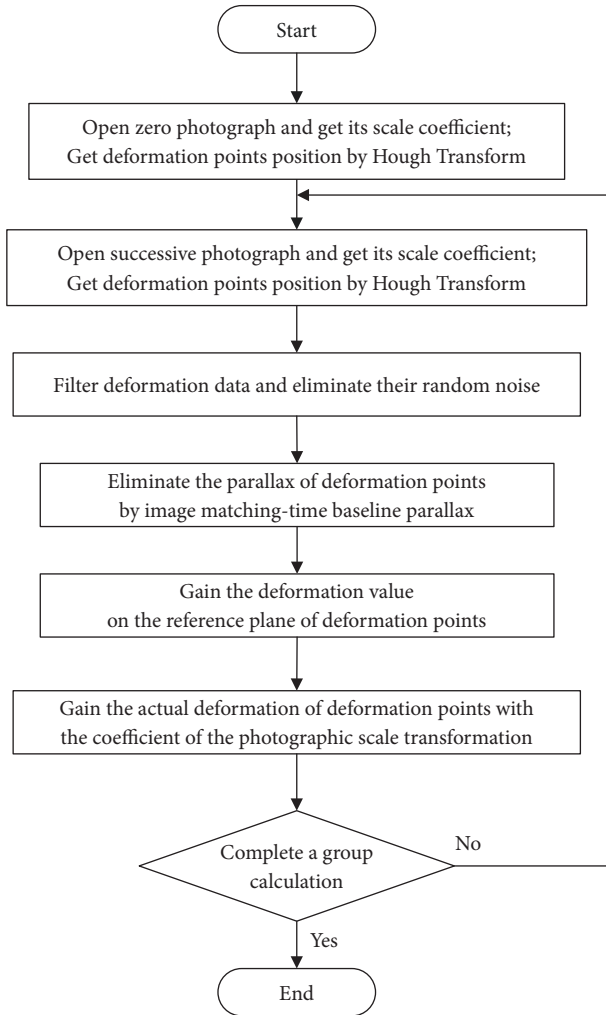


FIGURE 5: Flowchart of data processing.

(2.3m×1.5m×0.15cm) was put above the pit. The manganese steel plate, above which the masonry wall was built, hardly generated plastic deformation when impacted by the iron hammer due to its strong elasticity and strength. The impact hammer was a 25-kg iron cylinder (50cm in height and 12cm in diameter), whose upper portion was welded with an arc steel bar as a hook. Circular targets were uniformly distributed on the bricks of the masonry wall without obscuring the connections between the bricks, and the diameter was less than 53mm whenever possible.

Figure 6(b) illustrates an overlook of the test field, which shows the relative positions of the digital cameras and the masonry wall. In addition, awls were used to fix the steel plate in the test. The stakes were constructed at a stable place on both sides of the masonry wall, and reference points were laid on the stakes. Six Sony-350 digital cameras—the north and south sides of the masonry wall each with two cameras and the east and west sides each with only camera—were used to capture the instantaneous dynamic displacements of the masonry wall when the 25-kg hammer fell freely and hit the steel plate.

3.2. Test Process. As shown in Figure 7, we used a hammer to impact a steel plate to simulate the seismic oscillation. The test procedure is described as follows:

(1) The impact hammer was tied with a rope and lifted to a 0.3-meter position above the ground. Additionally, the digital cameras were adjusted to shoot the masonry wall clearly.

(2) Digital cameras shot the masonry wall to produce a zero image.

(3) Digital cameras shot the masonry wall when the 25-kg hammer fell freely and impacted the steel plate. One group test was completed.

(4) The impact hammer was tied with a rope and lifted to one of the following heights above the ground: 0.6 m, 0.9 m, 1.2 m, 1.5 m, 1.8 m, 2.1 m, 2.4 m, 2.7 m, 3.0 m, 3.3 m, 3.6 m, 3.9 m, 4.2 m, 4.5 m, 4.8 m, 5.1 m, 5.4 m, and 5.4 m, respectively. Repeat Step (3) for each height.

4. Numerical Simulation of Masonry Wall in Seismic Oscillation

As this study aims to simulate and analyze the failure process of a masonry wall and its crack development, a global continuous model was therefore adopted. Constitutive model of masonry material is based on Material Model 3: plastic kinematic model in LS-DYNA. In this study, the masonry wall was characterized by MU10-strength grade fired common brick, M7.5-strength grade mortar, material density of 1700kg/m³, elastic modulus of 2.704E9Pa, Poisson ratio 0.2, and compressive strength of 1.69MPa. Its bottom base was set to be rigid when we established a 3D (three-dimension) solid model of the masonry wall (Figure 8). Contact and collision were considered in the calculation, and we selected the Single Face, automatic single surface contact (ASSC), and set the static and dynamic friction coefficient to 0.1, and other parameters were the default values given by ANSYS. Then, we imposed horizontal seismic waves to influence the masonry wall; and the expression of a seismic wave used in this study is

$$\alpha = \sin(0.1t)(1 - \cos(0.02t)) * (\sin t + \sin(1.1t) + \sin(1.2t)) \quad (12)$$

where α is the acceleration of the seismic wave and t is the moment of seismic wave propagation.

5. Data Analysis and Discussion

5.1. Comparing the Results Obtained through the Field Test and the Numerical Simulation. After the masonry wall test, the masonry wall was damaged (Figure 9). The east-down masonry wall developed longitudinally through cracks (Line 1). Diagonal cracks (Line 2 and Line 3) emerged along the diagonal of the masonry wall. Crossing cracks (Line 4 and Line 5) occurred on the west of the masonry wall. Masonry damage was caused mainly by the shear stress created by the impact hammer. Cracks develop on a masonry wall when the shear stress is up to a certain extent. As shown in Figure 9(b), the stress concentration zones of the masonry wall were at its

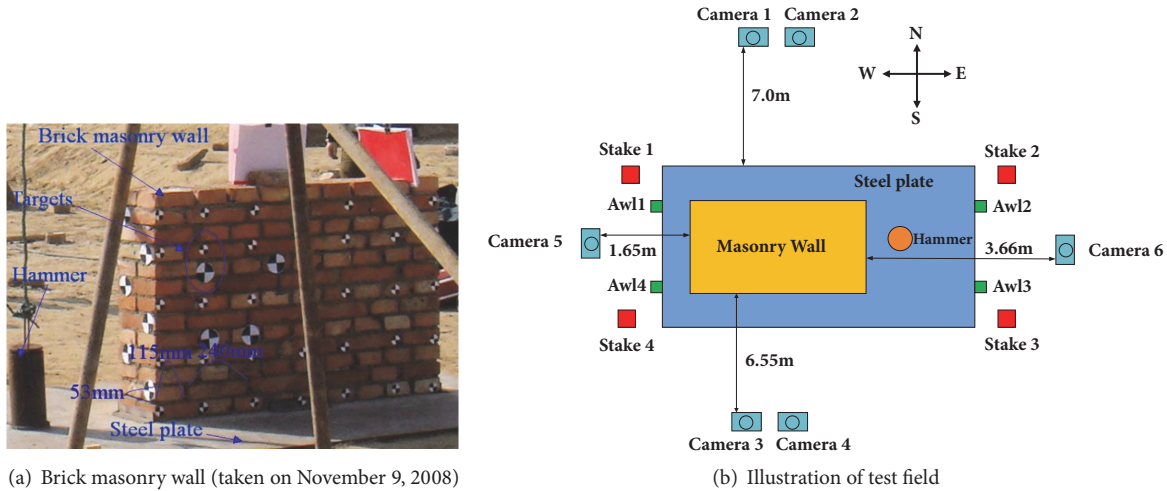


FIGURE 6: Test setup.

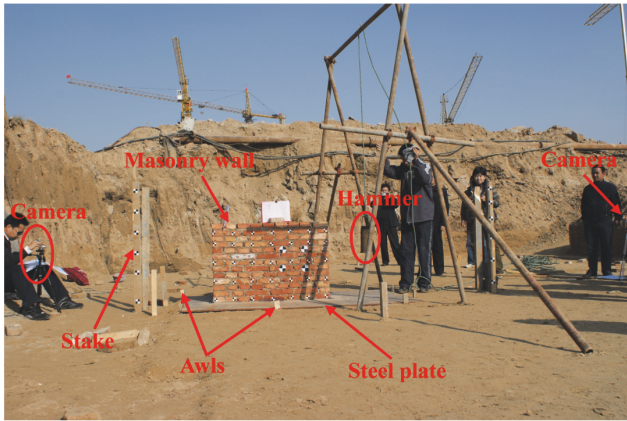


FIGURE 7: Monitoring a masonry wall in seismic oscillation in the field.

top left corner, top right corner, central region, two diagonals, and right side, and particularly at the bottom left corner. These stress concentration zones did develop cracks. For example, U33 and U34 in Figure 9(a) represent red zones in Figure 9(b), U0 represents the yellow zone in top right corner of the masonry wall, and Line 1 represents the turquoise zone on the right side of the masonry wall. These indicate that our test results are consistent with the numerical simulation, and that it is feasible to use the hammer to impact the suspended steel plate to simulate the seismic oscillation.

5.2. Analysis of Measurement Accuracy. Reference points were labeled as C0-C11 on stakes 3 and 4 of the masonry wall, and deformation points were labeled as U0-U38 on the south side of the masonry wall (Figure 10).

To assess the measurement accuracy of the PST-TBP method, we selected six reference points labeled as C0-C2 and C6-C8. In theory, these points do not move during the monitoring process, which means that their displacements should be zero. However, the displacements of these reference

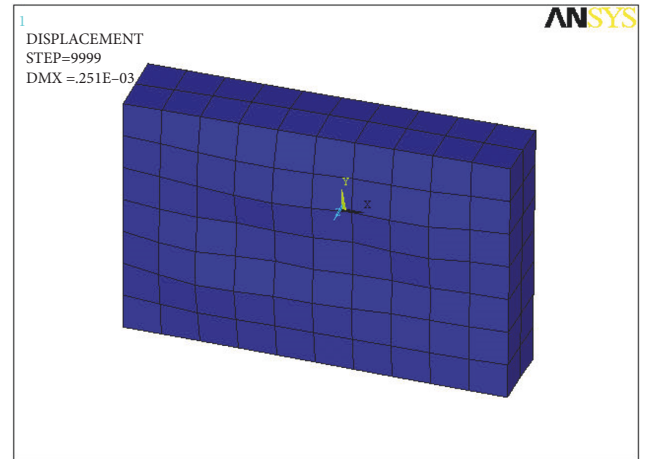


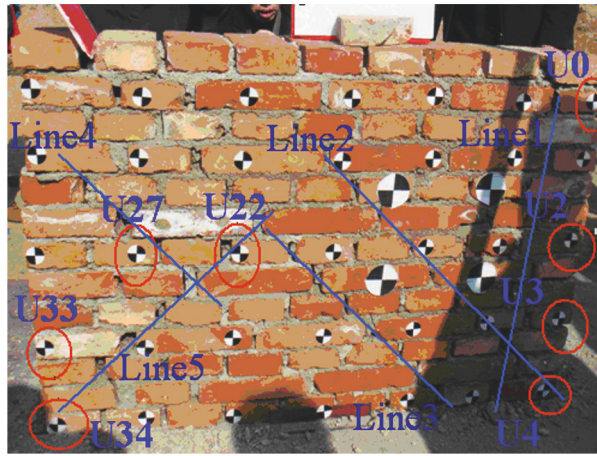
FIGURE 8: A 3D (three-dimension) solid model of the masonry wall, created in ANSYS.

TABLE 5: Measurement accuracy (/pixel) in the X-direction.

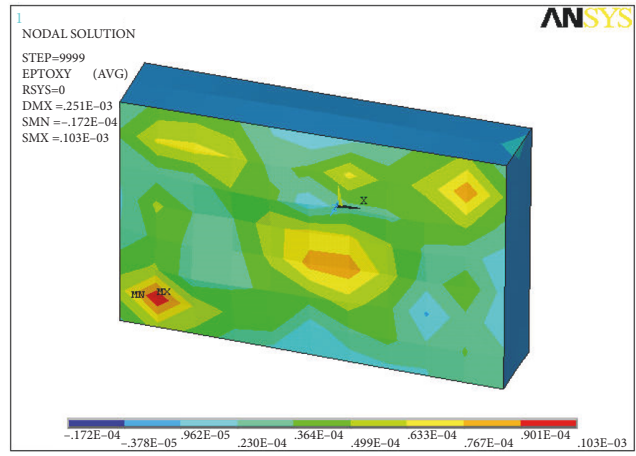
Point Name	C0	C1	C2	C6	C7	C8
Standard deviation	0.57	0.65	0.64	0.53	0.46	0.64
Average	0.58					

points obtained by the PST-TBP method were not zero. Their displacements can be considered as the measurement accuracy of the monocular digital photography used in this study. As the photographic scale is 1.43mm/pixel, Tables 5 and 6 show that the average measurement accuracy in the X- and Z-directions was 0.58 pixels (0.83 mm) and 0.59 pixels (0.84mm), respectively. In the west, the average measurement accuracy in the X- and Z-directions was 0.49mm and 0.44mm, respectively [33]. Thus, the PST-TBP method improves the measurement accuracy of a digital camera.

Note that in the DIC method, a suitable balance does exist between high spatial resolution and accuracy because the basic principle, the gray level distribution, of the DIC



(a) The masonry wall was damaged after the test



(b) Shear stress simulation with ANSYS

FIGURE 9: Masonry wall after seismic oscillation.

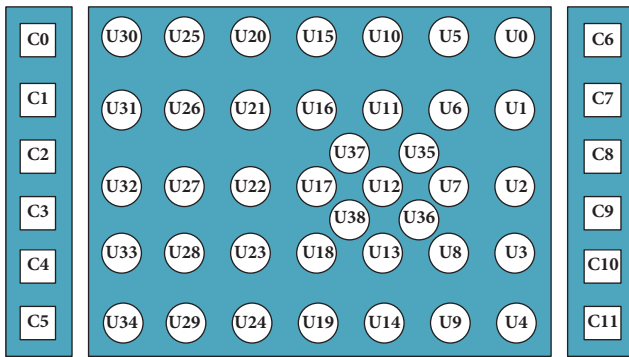


FIGURE 10: The distribution of selected monitoring points on the masonry wall and the stakes.

TABLE 6: Measurement accuracy (/pixel) in the Z-direction.

Point Name	C0	C1	C2	C6	C7	C8
Standard deviation	0.51	0.62	0.7	0.47	0.81	0.45
Average	0.59					

method decides that the tradeoff for enhanced accuracy is a reduced spatial resolution and the spatial resolution is the subset size [20]. However, the proposed method is based on the principle of the correspondence points matching. In our paper, the correspondence points are the reference points on the stakes. Once the position of the reference points and the camera are determined, the measurement accuracy of the PST-TBP method is determined. The measurement accuracy of the PST-TBP method increases with the camera resolution when the photographing distance is fixed and it has nothing to do with the spatial resolution (the subset size). The basic principles of these two methods are different in deal with the images. Thus, we cannot compare these two methods in terms of spatial resolution (the subset size), and in the proposed technique, there is no functional relationship between the

spatial resolution (the subset size) and the accuracy with reference to the DIC method.

The proposed method provides a new way to monitor the crack development of masonry wall in seismic oscillation by the PST-TBP (photographing scale transformation-time baseline parallax) method outside the laboratory. This paper aims to explore the feasibility of this new method. In our test, we did not use the DIC method to monitor the masonry wall in seismic oscillation. Thus, we cannot directly compare the proposed method with the DIC method in terms of measurement accuracy. We consulted the literature extensively to find the application of the DIC method outdoors. A few researchers, such as Küntz Michel and Tiago Ramos, have used the DIC method to monitor the engineering structures outside a laboratory. In their research, they did not mention the measurement accuracy of the DIC method outdoors. The DIC method is very sensitive to outdoors light conditions. The change of external light intensity has great influence on the measurement precision. Thus, the accuracy of the DIC method outside a laboratory is much lower than in a laboratory. However, there are no detailed data about the accuracy of the DIC method outside a laboratory. In the future test, we will use these two methods to monitor masonry walls in seismic oscillation to compare the proposed method with the DIC method with respect to accuracy.

5.3. *Masonry Wall Deformation Caused by S-Wave.* The seismic wave in the test is a body wave that consists of a P-wave (pressure wave) and an S-wave (shear wave). The shear wave can result in the shear deformation and the brittle fracture on a masonry structure. Furthermore, the S-wave is divided into an SH-wave (shear horizontal wave) and an SV-wave (shear vertical wave). Thus, this paper discusses the influence of the SH-wave and the SV-wave on the masonry wall based on test result.

5.3.1. *Masonry Wall Deformation Caused by an SH-Wave.* The SH-wave caused the masonry wall to move in the horizontal direction, which is perpendicular to the S-wave propagation.

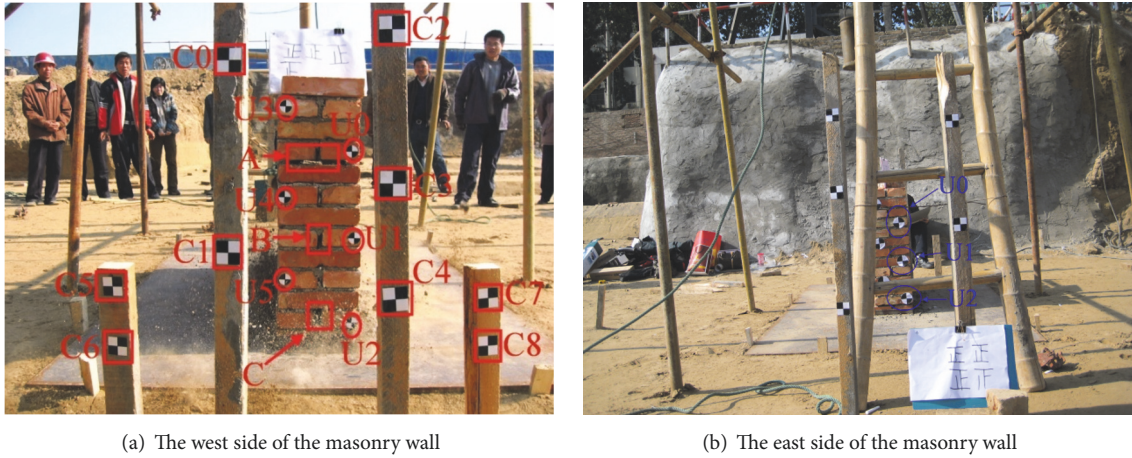


FIGURE 11: Both sides of the masonry wall.

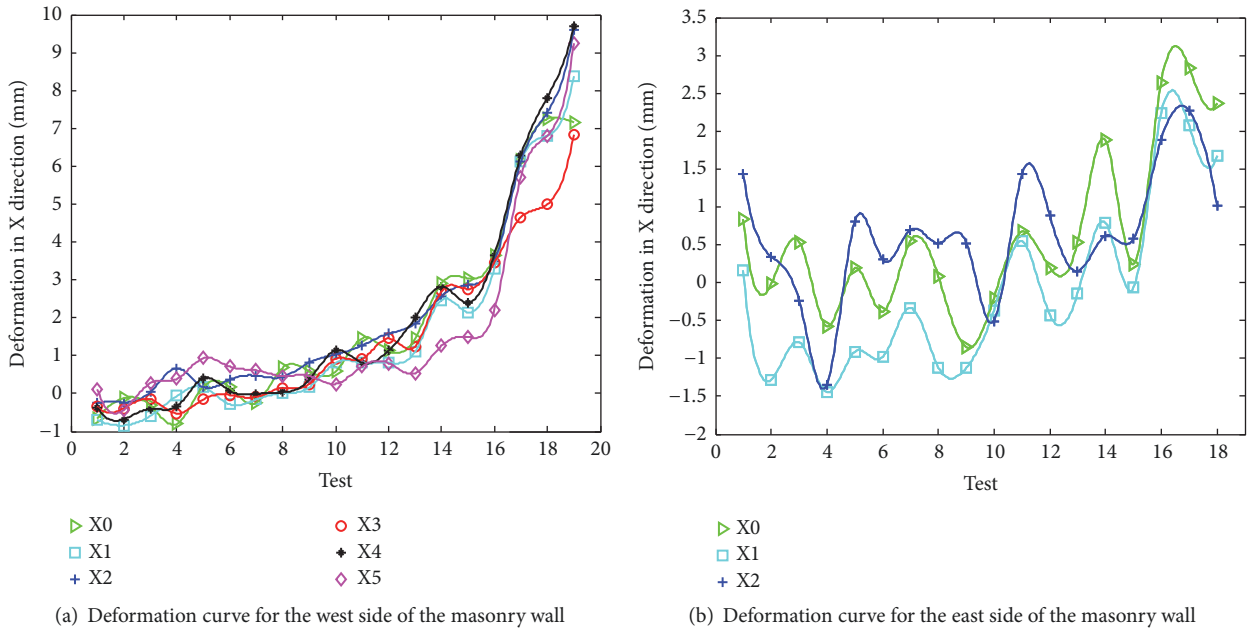


FIGURE 12: Deformation curve for the masonry wall.

We therefore chose the west and east sides of the masonry wall to examine the influence of the SH-wave on the masonry wall. As shown in Figure 11, the east side was near the hypocenter (the position impacted by the hammer), while the west side was far from the hypocenter. We drew deformation curves of the masonry wall for both sides to study the degree of damage along the direction of the SH-wave propagation (Figure 12). X0, X1, X2, X3, X4, and X5 in Figure 12 represent the displacements of U0, U1, U2, U3, U4, and U5 in the horizontal direction, respectively.

According to Figure 12, the displacements of the deformation points on the east side of the masonry wall were within the elasticity. There was a good integrity between the brick and the mud. However, plastic deformation occurred on the other side (i.e., the west side of the masonry wall), far from the hypocenter, with the increase in the intensity of the seismic

oscillation. The integrity between the brick and the mud was destroyed. The destruction from the SH-wave was gradually enhanced along its propagation direction.

5.3.2. Masonry Wall Deformation Caused by the SV-Wave. The SV-wave caused the masonry wall to move in the vertical direction which is perpendicular to S-wave propagation. To study the propagation characteristics of SV-wave in the masonry wall, we divided the masonry wall into five layers (Figure 13) and draw wave profile (Figure 14) of the deformation points for each layer.

Figure 14 shows that the displacements decreased gradually from east to west in the first and second layers and that the displacements fluctuated as sinusoid or cosine curves from east to west in the third, fourth, and fifth layers, particularly in the fifth layer in Figure 14(b). In conclusion, the SV-wave

TABLE 7: Maximum displacement differences (/mm) in the Z-direction between the adjacent layers.

Adjacent layers	U31-U32	U33-U34	U21-U22	U18-U19	U10-U11	U7-U8
Difference	4.31	6.02	3.15	4.33	3.06	2.65

TABLE 8: Relative deformation (/mm) in the X-direction.

Test	U34	U33	U27	U22	U21	U0	U3	U2	U4
15	-4.22	-5.7	-4.39	-1.6	2.65	3.76	2.45	2.4	1.07
16	-5.84	-8.69	-7.25	-1.53	2.79	4.18	4.14	2.72	-0.18
17	-3.98	-9.83	-7.17	-0.07	4.11	8.03	6.92	3.93	-0.13
18	-4.02	-9.77	-9.86	-1.32	4.39	8.44	7.05	5.6	1.34
19	-4.16	-10.3	-9.29	-0.67	6.1	8.71	9.79	6.51	1.58

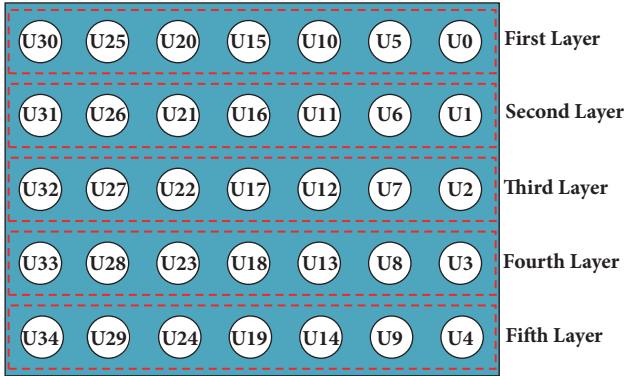


FIGURE 13: Layers on the masonry wall.

heavily affects not only the side near the hypocenter but also the third, fourth, and fifth layers of the masonry wall. In addition, we chose the displacement data of tests 16, 17, 18, and 19 to calculate the displacement differences between the adjacent layers. The maximum displacement differences between the adjacent layers are listed in Table 7. The figures show that the SV-wave destroyed the stability between some bricks and mud such as that between U31 and U32, U33 and U34, U21 and U22, U18 and U19, and U10 and U11. Then, the masonry wall developed cracks and brittle failure at these locations. Thus, the SV-wave is caused in the longitudinal through cracks on the side near the hypocenter and diagonal cracks along the diagonal of the masonry wall.

5.4. Crack Development of the Masonry Wall in Seismic Oscillation. In this section, the south and west sides of the masonry wall were selected to understand their crack development.

Figure 15 shows the positions of the deformation points on the south side of the masonry wall before (red) and after (blue) seismic oscillation tests. We reduced the scale of the masonry wall from (1200mm×800mm) to (60mm×80mm) to see the crack development of a masonry wall clearly. For narrative convenience, we defined that the X-direction is the position along the length of the masonry wall and that the Z-direction is the position along the height of the masonry wall. One point (X_0, Z_0) means that it is at position X_0

and Z_0 along the length and height of the masonry wall, respectively.

Figure 15 also clearly shows the direction of the movement of each point on the masonry wall. The crack development is therefore determined by the relative movement of the adjacent deformation points. For example, in Figure 15(b) point (0, 60) moves to the right, and point (0, 40) moves to the left; therefore, cracks will develop between point (0, 60) and point (0, 40). In Figure 15(a), point (0, 20) moves 8.69mm to the left, and point (10, 20) moves 2.97mm to the left. The displacement difference between them was 5.72mm, and the cracks therefore will develop between them.

For clearly understanding the relationship between the seismic wave propagation and the crack development of the masonry wall, the following deformation points around the crack attract our attention, U0, U2, U3, U4, U21, U22, U27, U33, and U34. As tests 15 to 19 cause the masonry wall to be destroyed gradually, we selected their displacement data (Tables 8 and 9) to study. Then, Figure 16 was drawn based on these displacement data.

In Figure 16(a), it is surprising that the shape of the wave profile of the cracks in the X-direction is very similar to a sinusoid or a cosine curve. The similarity increases with the seismic oscillation intensity. This phenomenon is consistent with the results from a shaking table [20] and further suggests that it is feasible to simulate the seismic oscillation by using a hammer to impact a suspended steel plate. In Figure 16(b), wave profiles of the cracks in the Z-direction are of good volatility. They fluctuated up and down around a horizontal line, which conforms to the characteristics of the seismic wave propagation. Wave profiles of the cracks therefore represent the relationship between the crack development of the masonry wall and the seismic wave propagation well.

On the west, we depicted deformation curves of deformation points. Figure 17(a) shows that the maximal displacement difference for the obvious horizontal crack developed between U0 and U4 is 2.56 mm, while Figure 17(b) shows that maximal displacement difference for the obvious vertical crack developed between U0 and U4 is 4.31 mm. Moreover, slight horizontal cracks developed on the position between U2 and U5 and the position between U1 and U4. These findings are consistent with the destroyed masonry wall (Figure 11(a)). Position A (Figure 11(a)) developed obvious vertical and horizontal cracks, and position B and C

TABLE 9: Relative deformation (/mm) in the Z-direction.

Test	U34	U33	U27	U22	U21	U0	U3	U2	U4
15	8.7	4.15	6.76	6.77	5.09	7.8	7.03	6.77	7.27
16	9.2	4.67	5.83	7.23	5.57	9.58	8.75	7.08	8.98
17	9.34	5.01	5.09	6.63	5.17	9.85	8.48	8.46	8.5
18	11.71	5.69	6.79	9.61	6.46	10.39	9.7	10.85	9.98
19	12.45	7.86	7.59	7.61	7.33	11.51	9.38	10.54	11.09

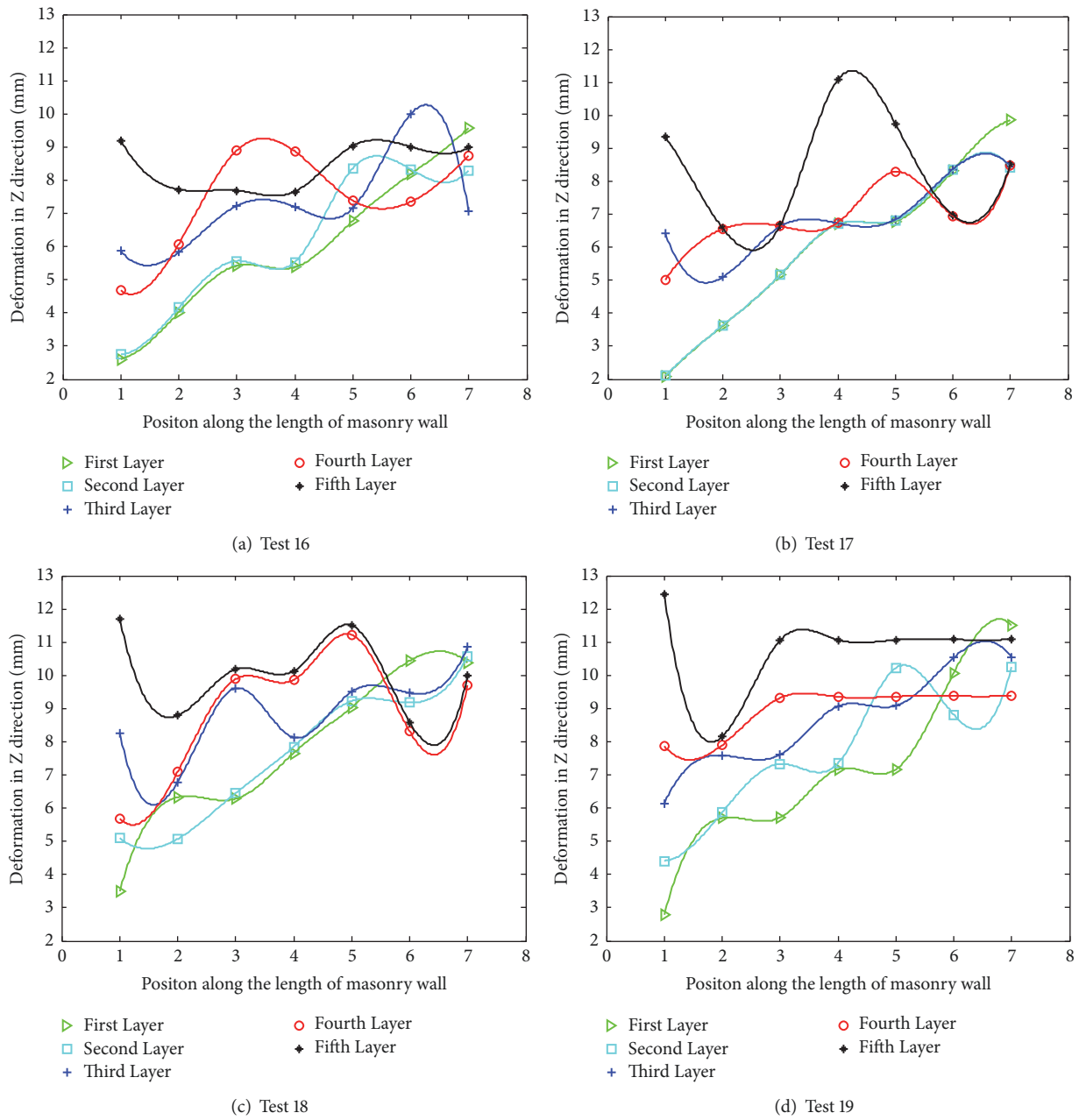


FIGURE 14: Wave profile of SV-wave in each layer.

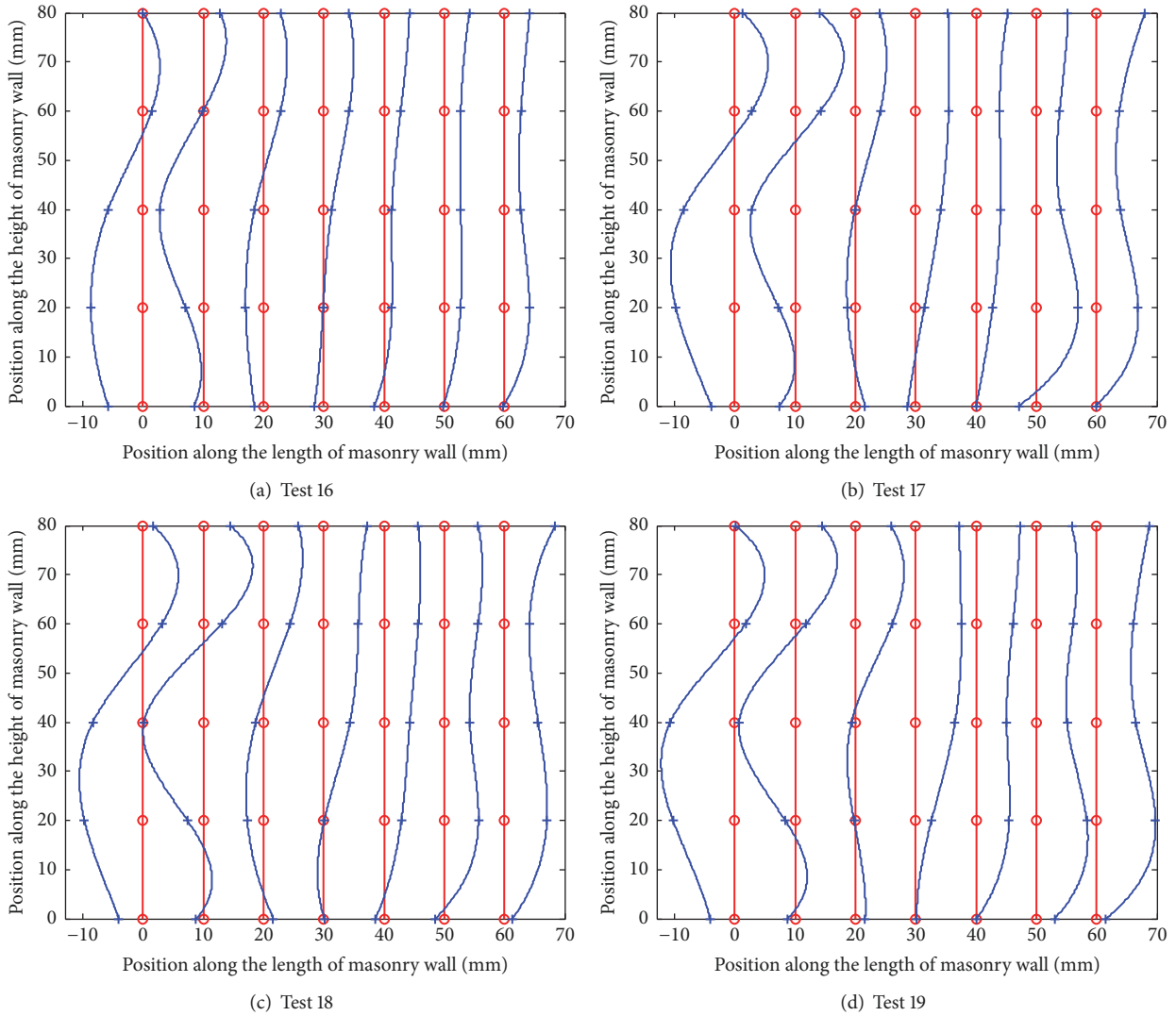


FIGURE 15: Positions of deformation points before and after seismic oscillation test.

developed slight horizontal cracks. In addition, the crack on C occurred in test 14, the vertical and horizontal cracks on A occurred in test 16 and 19, respectively, and the crack on B occurred in test 19. Thus, in seismic oscillation the shear failure first develops in the middle-lower portion of a masonry wall. Then, the bonding between the bricks and the mud is invalid in the middle-upper portion of a masonry wall. Last, shear failure occurs in the middle of a masonry wall.

Based on the test results, we propose some preliminary suggestions to reinforce a masonry wall. Figure 18 shows that construction columns 1 and 2 are set on the two sides of a masonry wall to prevent slip failure, and solid piers 1 and 2 replace the initial bricks easily damaged by the SH-wave, and solid flagstones 1 and 2 replace the initial bricks to minimize the SV-wave influence on the masonry wall.

Note that in the field we used a hammer to impact a suspended steel plate to simulate seismic oscillation. There is no comparative study with reference to this methodology demonstrated elsewhere in the reported research. However, it is feasible as some test phenomena are consistent with

the results from numerical simulation and shaking tables. Moreover, the suggestions for reinforcing the masonry walls are restricted to the test example in this study, and future tests are required to prove their feasibility.

6. Conclusions

This study proposes a new technique to study masonry walls in seismic oscillation outdoors. In this technique, a freely falling hammer impacts a suspended steel plate to simulate seismic oscillation propagated in a masonry wall outdoors. Then, we used monocular digital photography based on the (PST-TBP) (photographing scale transformation-time baseline parallax) method to monitor the crack development of the masonry wall outdoors. In addition, the field test results are also compared with the simulation results produced by ANSYS. The following conclusions are provided:

(1) It is feasible to use a hammer to impact a suspended steel plate to simulate seismic oscillation in the field. Stress concentration zones simulated by ANSYS are consistent with

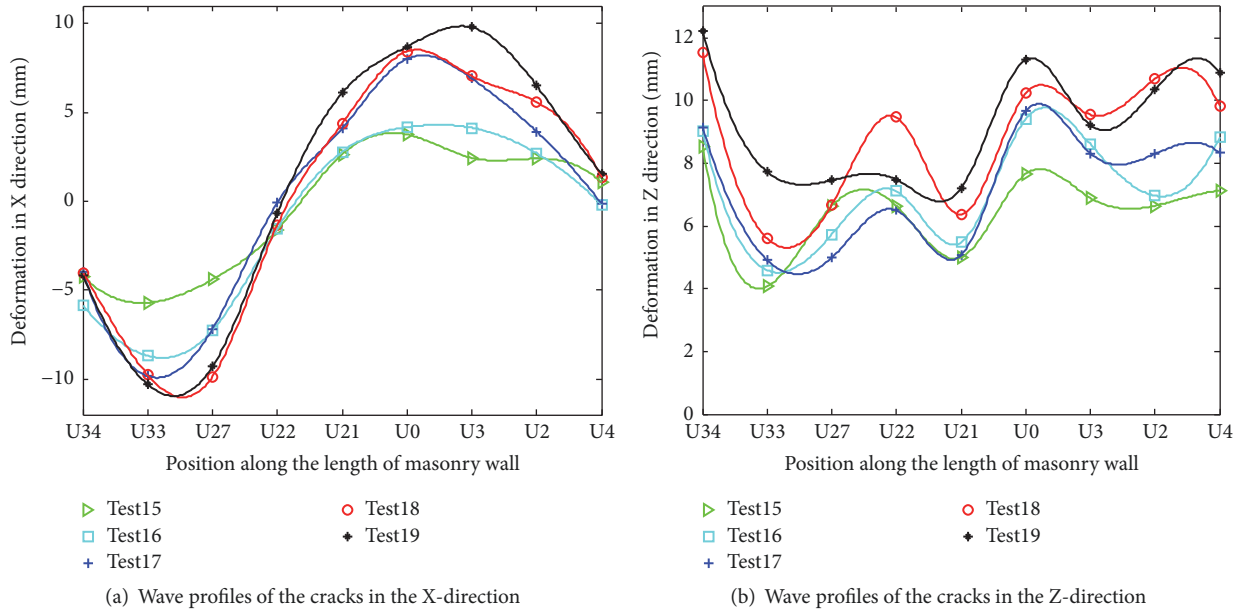


FIGURE 16: Wave profile of the cracks.

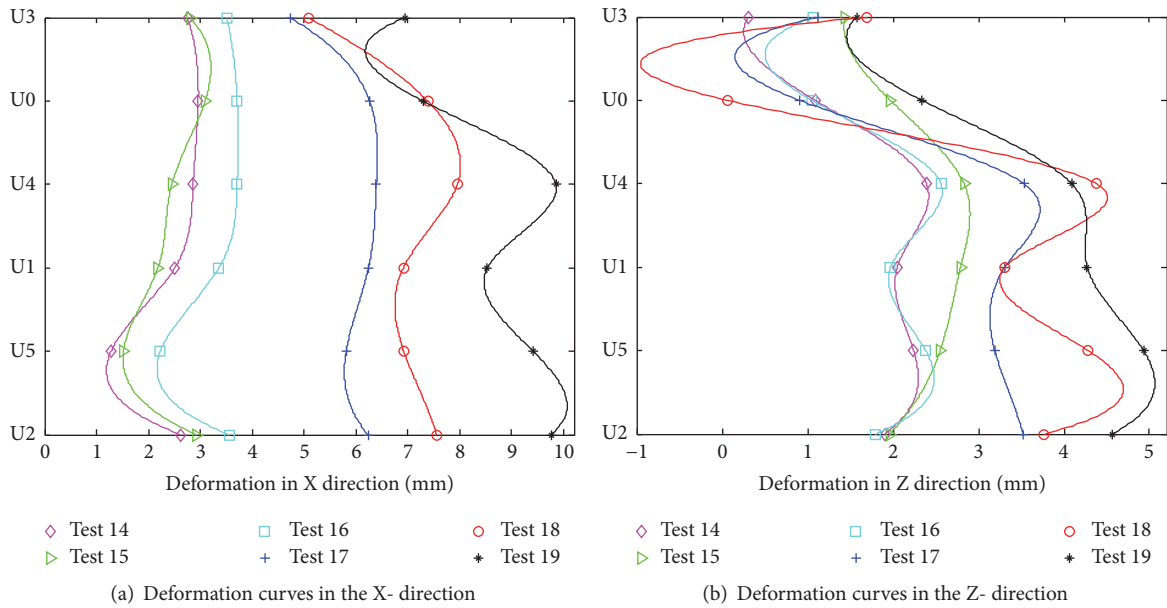


FIGURE 17: Deformation curves for the west side of the masonry wall.

the crack development positions of the destroyed masonry wall. The shape of the wave profile of the cracks in the horizontal direction is very similar to a sinusoid or cosine curve. This phenomenon agrees with the test results from a shaking table.

(2) Monocular digital photography based on the PST-TBP method can meet the accuracy requirement to monitor masonry walls in seismic oscillation outdoors. The average measurement accuracies of Camera 3 in the X- and Z-directions are 0.83 mm and 0.84 mm, respectively. The average measurement accuracies of Camera 5 in the X- and Z-directions are 0.49 mm and 0.44 mm, respectively.

(3) Diagonal cracks and longitudinal through cracks may occur along the diagonal of a masonry wall and on the side near the hypocenter, respectively. The destruction from the SH-wave is gradually enhanced along its propagation direction. Cracks may occur on the side of a masonry wall far from the hypocenter due to SH-waves. SV-waves seriously affect the central bottom portion of a masonry wall without decreasing intensity, but they affect the upper portion of a masonry wall with decreasing intensity from the position near the hypocenter to the position far from the hypocenter.

(4) The crack development pattern of a masonry wall in seismic oscillation is consistent with the seismic wave

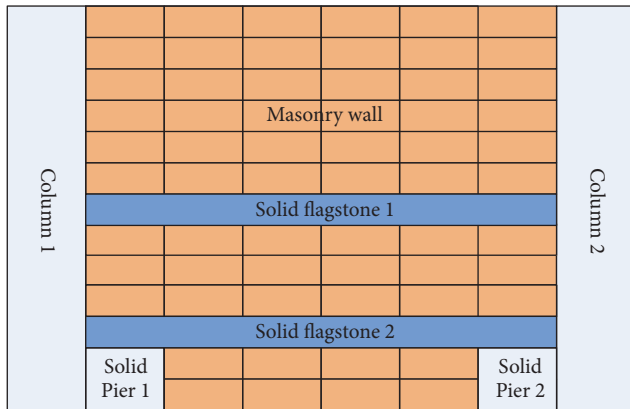


FIGURE 18: Illustration of masonry wall reinforcement.

propagation because the shape of the wave profile of the cracks in the horizontal direction is very similar to a sinusoid or a cosine curve.

This study used monocular digital photography based on the PST-TBP method to conduct innovative research into the relationship between crack development and seismic wave propagation on the masonry wall and provides a technical basis to monitor instantaneous dynamic displacements of masonry structures in seismic oscillation outdoors to warn of possible danger. This study also has significant implications for improved construction of masonry structures in earthquake-prone areas.

Data Availability

The data used to support the findings of this study are available from the corresponding author upon request.

Conflicts of Interest

The authors declare that there are no conflicts of interest regarding the publication of this paper.

Acknowledgments

The study was supported by the National Natural Science Foundation of China (Grant no. 51674249) and the Science and Technology Project of Shandong Province, China (Grant no. 2010GZX20125). The authors thank the management department of a construction site in Liaocheng City (Shandong) for authorizing their fieldwork and thank Su LIU for the numerical simulation in the study.

References

- [1] C. J. Xu, Q. B. Fan, Q. Wang, S. M. Yang, and G. Y. Jiang, "Postseismic deformation after 2008 wenchuan earthquake," *Survey Review*, vol. 46, no. 339, pp. 432–436, 2014.
- [2] P. Cui, X.-Q. Chen, Y.-Y. Zhu et al., "The Wenchuan Earthquake (May 12, 2008), Sichuan Province, China, and resulting geohazards," *Natural Hazards*, vol. 56, no. 1, pp. 19–36, 2011.
- [3] S. Tung, M. Shih, and W. Sung, "Development of digital image correlation method to analyse crack variations of masonry wall," *Sadhana*, vol. 33, no. 6, pp. 767–779, 2008.
- [4] D. P. Abrams and T. J. Paulson, "Modeling earthquake response of concrete masonry building structures," *ACI Structural Journal*, vol. 88, no. 4, pp. 475–485, 1991.
- [5] A. Hillerborg, M. Mod er, and P.-E. Petersson, "Analysis of crack formation and crack growth in concrete by means of fracture mechanics and finite elements," *Cement and Concrete Research*, vol. 6, no. 6, pp. 773–781, 1976.
- [6] P. Bocca, A. Carpinteri, and S. Valente, "Fracture mechanics of brick masonry: size effects and snap-back analysis," *Materials and Structures*, vol. 22, no. 5, pp. 364–373, 1989.
- [7] M. Giaretton, D. Dizhur, and J. M. Ingham, "Dynamic testing of as-built clay brick unreinforced masonry parapets," *Engineering Structures*, vol. 127, pp. 676–685, 2016.
- [8] H.-G. Maas and U. Hampel, "Programmetric techniques in civil engineering material testing and structure monitoring," *Photogrammetric Engineering and Remote Sensing*, vol. 72, no. 1, pp. 39–45, 2006.
- [9] R. N. Jiang, D. V. J uregui, and K. R. White, "Close-range photogrammetry applications in bridge measurement: literature review," *Measurement*, vol. 41, no. 8, pp. 823–834, 2008.
- [10] G. Abdelsayed, B. Bakht, and L. G. Jaeger, "Soil-steel bridges: design and construction," *Conduits*, 1993.
- [11] C. Forno, S. Brown, R. A. Hunt, A. M. Kearney, and S. Oldfield, "Measurement of deformation of a bridge by Moir  photography and photogrammetry," *Strain*, vol. 27, no. 3, pp. 83–87, 2008.
- [12] Y. Chen, "Detection Technology of Structural Cracks Amplification Digital Photograph and Real-time Transmission," *Construction Quality*, 2012.
- [13] D. Lecompte, J. Vantomme, and H. Sol, "Crack detection in a concrete beam using two different camera techniques," *Structural Health and Monitoring*, vol. 5, no. 1, pp. 59–68, 2006.
- [14] M. K untz, M. Jolin, J. Bastien, F. Perez, and F. Hild, "Digital image correlation analysis of crack behavior in a reinforced concrete beam during a load test," *Canadian Journal of Civil Engineering*, vol. 33, no. 11, pp. 1418–1425, 2006.
- [15] J.-F. Destrebecq, E. Toussaint, and E. Ferrier, "Analysis of cracks and deformations in a full scale reinforced concrete beam using a digital image correlation technique," *Experimental Mechanics*, vol. 51, no. 6, pp. 879–890, 2011.
- [16] B. Ghiassi, J. Xavier, D. V. Oliveira, and P. B. Louren o, "Application of digital image correlation in investigating the bond between FRP and masonry," *Composite Structures*, vol. 106, pp. 340–349, 2013.
- [17] T. Ramos, A. Furtado, S. Eslami et al., "2D and 3D digital image correlation in civil engineering - measurements in a masonry wall," *Procedia Engineering*, vol. 114, pp. 215–222, 2015.
- [18] H.-L. Nghiem, M. Al Heib, and F. Emeriault, "Method based on digital image correlation for damage assessment in masonry structures," *Engineering Structures*, vol. 86, pp. 1–15, 2015.
- [19] A. H. Salmanpour and N. Mojsilovic, "Application of Digital Image Correlation for strain measurements of large masonry walls," in *Proceedings of the Asia Pacific Congress on Computational Mechanics*, 2013.
- [20] R. Ghorbani, F. Matta, and M. A. Sutton, "Full-Field Deformation Measurement and Crack Mapping on Confined Masonry Walls Using Digital Image Correlation," *Experimental Mechanics*, vol. 55, no. 1, pp. 227–243, 2015.

- [21] B. Ghiassi, J. Xavier, D. V. Oliveira, A. Kwiecien, P. B. Lourenço, and B. Zajac, "Evaluation of the bond performance in FRP-brick components re-bonded after initial delamination," *Composite Structures*, vol. 123, pp. 271–281, 2015.
- [22] Z. Guojian, L. Shengzhen, Z. Tonglong, and Y. Chengxin, "Exploring of PST-TBPM in Monitoring Bridge Dynamic Deflection in Vibration," in *Proceedings of the IOP Conference Series: Earth and Environmental Science*, vol. 108, 2018.
- [23] C. Mingzhi, Z. Yongqian, H. Hua, Y. Chengxin, and Z. Guojian, "Exploring of PST-TBPM in Monitoring Dynamic Deformation of Steel Structure in Vibration," in *Proceedings of the IOP Conference Series: Earth and Environmental Science*, vol. 108, 2018.
- [24] C. Mingzhi, Y. ChengXin, X. Na, Z. YongQian, and Y. WenShan, "Application study of digital analytical method on deformation monitor of high-rise goods shelf," in *Proceedings of the IEEE International Conference on Automation and Logistics*, pp. 2084–2088, 2008.
- [25] G. Zhang, S. Liu, T. Zhao, and C. Yu, "Exploring of PST-TBPM in Monitoring Bridge Dynamic Deflection in Vibration," in *Proceedings of the IOP Conference Series: Earth and Environmental Science*, 2018.
- [26] R. R. P. D. Samuel, *Close-Range Photogrammetry*, Springer, Berlin, Germany, 2014.
- [27] K. Fujimoto, J. Sun, H. Takebe, M. Suwa, and S. Naoi, "Shape from parallel geodesics for distortion correction of digital camera document images," *Journal of Electronic Imaging*, pp. 286–290, 2007.
- [28] H. Yanagi and H. Chikatsu, "Factors and estimation of accuracy in digital close range photogrammetry using digital cameras," *Journal of the Japan society of photogrammetry*, vol. 50, no. 1, pp. 4–17, 2011.
- [29] X. U. Fang, *The Monitor of Steel Structure Bend Deformation Based on Digital Photogrammetry*, Editorial Board of Geomatics & Information Science of Wuhan University, 2001.
- [30] J. I. Jeong, S. Y. Moon, S. G. Choi, and D. H. Rho, "A study on the flexible camera calibration method using a grid type frame with different line widths," in *Proceedings of the Sice Conference*, vol. 2, pp. 1319–1324, 2002.
- [31] M.-C. Lu, C.-C. Hsu, and Y.-Y. Lu, "Distance and angle measurement of distant objects on an oblique plane based on pixel variation of CCD image," in *Proceedings of the 2010 IEEE International Instrumentation and Measurement Technology Conference, I2MTC 2010*, pp. 318–322, Austin, TX, USA, May 2010.
- [32] C.-C. J. Hsu, M.-C. Lu, and Y.-Y. Lu, "Distance and angle measurement of objects on an oblique plane based on pixel number variation of CCD images," *IEEE Transactions on Instrumentation and Measurement*, vol. 60, no. 5, pp. 1779–1794, 2011.
- [33] G. Zhang, C. Yu, and X. Ding, "Analyzing crack development pattern of masonry structure in seismic oscillation by digital photography," in *Proceedings of the IOP Conference Series: Earth and Environmental Science*, vol. 108, 2018.
- [34] Y. Sun, H. Yang, and S. Jiang, "Evaluation of seismic performance and tolerant deformation on existing brick masonry buildings," *Shenyang Jianzhu Daxue Xuebao*, vol. 29, no. 5, pp. 861–867, 2013.
- [35] Ministry of Housing and Urban-Rural Development of the people's Republic, *Code for Design of Masonry Structures*, China Building Industry Press, 2011.
- [36] Y. Zhao, Y. Wu, and C. Yu, "Research on Instantaneous Dynamical Deformation Monitoring the Masonry Structure Based on Artificial Earthquake Motion," *International Journal of Hybrid Information Technology*, vol. 8, no. 10, pp. 241–252, 2015.



Hindawi

Submit your manuscripts at
www.hindawi.com

